Cell

A Deeper Look into Translation Initiation

Andrei A. Korostelev[1,*]
[1]RNA Therapeutics Institute, Department of Biochemistry and Molecular Pharmacology, University of Massachusetts Medical School, 368 Plantation Street, Worcester, MA 01605, USA
*Correspondence: andrei.korostelev@umassmed.edu
http://dx.doi.org/10.1016/j.cell.2014.10.005

Eukaryotic translation initiation requires coordinated assembly of a remarkable array of initiation factors onto the small ribosomal subunit to select an appropriate mRNA start codon. Studies from Erzberger et al. and Hussain et al. bring new insights into this mechanism by looking at early and late initiation intermediates.

Initiation is a key step of translation, resulting in the precise placement of an initiation AUG codon into the ribosome, thereby establishing the correct open reading frame of an mRNA for protein synthesis. Bacterial translation initiation is conceptually simple, relying on a Shine-Dalgarno sequence upstream of an initiation codon to anchor the mRNA to the small ribosomal subunit and three initiation factors to help recruit the initiator tRNA and fend off elongator tRNAs and the large subunit until the initiator tRNA clicks into the P (peptidyl) site. In eukaryotes, however, initiation is an intricate process that requires at least a dozen initiation factors (reviewed in Hinnebusch and Lorsch, 2012; Jackson et al., 2010). Two new studies provide an unprecedented level of insight into this process (Erzberger et al., 2014; Hussain et al., 2014)

The major challenges in studying translation initiation structurally are the number of steps and the size of the complexes involved and the intricate choreography of conformational changes required to scan for the proper start codon and act on it. Some initiation factors are multisubunit complexes, such as the ~750 kDa mammalian initiation factor 3 (eIF3) composed of 13 proteins. Assembly of the translation initiation complex on the small 40S ribosomal subunit occurs in a stepwise fashion. The 40S•eIF3 particle (Figure 1A) bound with eukaryotic initiation factors eIF1, eIF1A, and eIF5 recruits the methionine initiator tRNA (Met-tRNA$_i$) attached to GTP-bound eIF2. This 43S pre-initiation complex (Figure 1B) then associates with an mRNA whose 7-methylguanosine 5′ cap has been recognized by the eIF4F multiprotein factor. The 43S particle scans the mRNA in the 5′-to-3′ direction until it finds a start codon in an appropriate sequence context. Met-tRNA$_i$ then base pairs with the AUG codon in the P site of the small subunit, forming the 48S initiation complex (Figure 1C). Joining with the 60S ribosomal subunit completes the formation of the 80S ribosome that is ready to proceed with protein synthesis.

Two recent reports of molecular structures of eukaryotic initiation complexes help to unveil several important aspects of the initiation mechanism (Erzberger et al., 2014; Hussain et al., 2014). Erzberger and colleagues report a structure of yeast eIF3 bound to the 40S ribosomal subunit in a complex with eIF1, representing an early intermediate in translation initiation. In accordance with its large size, eIF3 is considered to be a "master regulator" of initiation, mediating interactions with many initiation factors, promoting mRNA recruitment and scanning, and preventing premature association of the initiation complex with the large ribosomal subunit (Hinnebusch and Lorsch, 2012; Jackson et al., 2010). In yeast, eIF3 contains six proteins—eIF3a, eIF3b, eIF3c, eIF3g, eIF3i, and eIF3j—which are highly conserved and form the core of eIF3 in all eukaryotes. Based on biochemical and cryo-EM studies, eIF3 is associated with the solvent-exposed surface (the "back") of the small ribosomal subunit (Hashem et al., 2013 and references therein). Due to the dynamic nature of eIF3 and the lack of high-resolution structural information for the complex, assigning the position of each eIF3 subunit on the 40S subunit has been a challenge.

To tackle this problem, Erzberger and colleagues employed a hybrid, multi-technique approach. First, they determined high-resolution crystal structures of isolated eIF3 subunits, namely eIF3a, the eIF3a•eIF3c dimer, the eIF3b core, and eIF3i bound with the terminal domains of eIF3b and eiF3g. Next, using a combination of negative-stain electron microscopy and crosslink mass-spectrometry, the authors provided a detailed view of the interactions and organization of eIF3 in the 40S•eIF1•eIF3 complex. As an internal control, intra-40S protein crosslinks revealed interactions consistent with those predicted from the 40S crystal structure, demonstrating the robustness of the crosslinking approach. Analysis of 90,000 possible crosslink-restrained structural models of the 40S•eIF1•eIF3 complex converged on a final cluster of solutions in which the position of each eIF3 subunit on the surface of the 40S subunit is assigned with high confidence and agrees with crystallographic and electron-microscopy data. These analyses reveal that eIF3 forms a horseshoe-like structure, embracing the 40S subunit (Figure 1A). The eIF3 subunits intertwine, bridging the mRNA entrance and exit tunnels near the A and E sites, respectively, agreeing with previous structural, genetic, and biochemical data (reviewed in Hinnebusch, 2014). The model provides a framework for future studies and represents a major step toward elucidating how eIF3 orchestrates many aspects of initiation by reaching out to the binding sites of other initiation factors in the 43S preinitiation complex as well as interacting with the mRNA at both the entrance and exit tunnels in the 43S•mRNA complex.

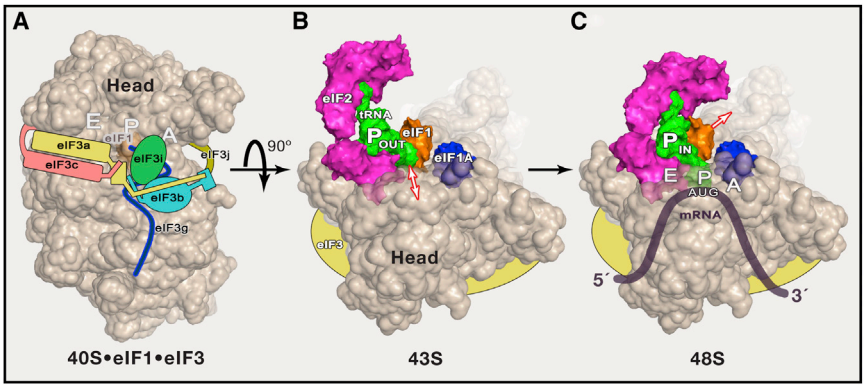

Figure 1. Schematic of 48S Initiation Complex Formation and Architecture

(A) Location of subunits of initiation factor eIF3 on the solvent surface of the 40S subunit, as revealed by Erzberger et al. (2014). A (aminoacyl), P (peptidyl), and E (exit) sites of tRNA binding and the location of eIF1 (brown) on the intersubunit surface are labeled.

(B) Schematic view of the 43S preinitiation complex formed prior to mRNA recruitment, inferred from the structure of a partial mammalian 43S complex (Hashem et al., 2013). The schematic was rendered using the structures of the 40S•eIF1•eIF1A complex (PDB ID 4BPE) and archaeal aIF2•GDPNP•Met-tRNA$_i$ ternary complex (PDB ID 3V11).

(C) Partial 48S initiation complex with Met-tRNA$_i$ fully accommodated and base paired with the AUG start codon, as revealed in the 4 Å cryo-EM structure by Hussain et al. (2014). The putative location of eIF5 (behind eIF2 in this view) is not shown.

Initiation involves scanning by the 43S complex to search for a start codon. A recent cryo-EM study of a partial mammalian 43S particle, formed in the absence of mRNA (Figure 1B), found that the initiator tRNA is located ~7 Å outside of the P site (Hashem et al., 2013), consistent with a state (P_{OUT}) that allows mRNA to load and/or bypass during scanning. In new work, Hussain and colleagues (2014) report a 4 Å cryo-EM structure of a partial yeast 48S initiation complex, formed downstream of the 40S•eIF3 and 43S complexes (Figures 1A and 1B). This structure reveals rearrangements and interactions in the initiation complex upon arrival of an AUG codon in the P site (Figure 1C). Although eIF3 was not captured, the structure offers the highest-resolution view to date of the mRNA, eIF2•GTP•Met-tRNA$_i$ ternary complex, eIF1A, eIF1, and the putative location of eIF5 in the 48S complex.

As previously observed in a low-resolution crystal structure of a 48S-like initiation complex formed in the absence of eIF1 and eIF2 (Lomakin and Steitz, 2013), the anticodon stem loop of Met-tRNA$_i$ in the new cryoEM structure is fully accommodated in the P site (P_{IN}) and base paired with the AUG codon. The conformation of the tRNA as a whole, however, is different between the two structures, suggesting that eIF2 and likely other initiation factors properly orient the tRNA in the 48S complex. Interestingly, eIF1 remains bound next to the P site rather than being forced out by steric hindrance with tRNA, as expected from biochemical (Hinnebusch and Lorsch, 2012; Jackson et al., 2010) and structural work (Lomakin and Steitz, 2013; Rabl et al., 2011). As eIF1 is slightly distorted and displaced by tRNA from its position, this new structure represents an intermediate state that is sampled just prior to dissociation of eIF1.

The structure presented in Hussain et al. also provides new insight into the roles of eIF2 and eIF1A in start codon selection. The most efficient initiation site is an AUG codon in the context of the Kozak consensus sequence (Kozak, 1986), a purine residue at position −3 relative to the +1 adenosine of the AUG and a guanosine at position +4. Cross-linking experiments and recent cryo-EM structures of 80S•tRNA•mRNA complexes (Svidritskiy et al., 2014 and references therein) suggest that interactions in the ribosomal E site between the −3 purine, 18S ribosomal RNA, and protein rpS5 (uS7) help position the AUG codon in the P site. Based on their 48S-like structure, Lomakin and Steitz (2013) proposed that the nucleotide at position +4 in the A site is "sensed" by the N-terminal tail of eIF1A, although the details of this communication remained unresolved. Now the structure by Hussain et al. provides a detailed view of mRNA interactions, including uS7 and a conserved loop of eIF2 contacting the mRNA at the position −3, and the N-terminal tail of eIF1A interacting directly with nucleotide +4, thus suggesting how initiation factors might examine the start-codon context during scanning.

In summary, complementary work by Erzberger et al. (2014) and Hussain et al., 2014 provides a deeper view into translation initiation by presenting a detailed picture of the interplay between initiation factors, tRNA, mRNA, and the 40S subunit in an early and late initiation states. The next frontier is to reveal structural mechanisms of the intermediate steps, including recruitment of eIF4F-bound mRNA onto the 43S preinitiation complex and scanning of the 5′ untranslated region of the mRNA by the 43S complex and associated helicases.

REFERENCES

Erzberger, J.P., Stengel, F., Pellarin, R., Zhang, S., Schaefer, T., Aylett, C.H., Cimermančič, P., Boehringer, D., Sali, A., Aebersold, R., and Ban, N. (2014). Cell *158*, 1123–1135.

Hashem, Y., des Georges, A., Dhote, V., Langlois, R., Liao, H.Y., Grassucci, R.A., Hellen, C.U., Pestova, T.V., and Frank, J. (2013). Cell *153*, 1108–1119.

Hinnebusch, A.G. (2014). Annu. Rev. Biochem. *83*, 779–812.

Hinnebusch, A.G., and Lorsch, J.R. (2012). Cold Spring Harb. Perspect. Biol. *4*. Published online July 18, 2012. http://dx.doi.org/10.1101/cshperspect.a011544.

Hussain, T., Llácer, J.L., Fernández, I.S., Munoz, A., Martin-Marcos, P., Savva, C.G., Lorsch, J.R., Hinnebusch, A.G., and Ramakrishnan, V. (2014). Cell *159*, this issue, 597–607.

Jackson, R.J., Hellen, C.U., and Pestova, T.V. (2010). Nat. Rev. Mol. Cell Biol. *11*, 113–127.

Kozak, M. (1986). Cell *44*, 283–292.

Lomakin, I.B., and Steitz, T.A. (2013). Nature *500*, 307–311.

Rabl, J., Leibundgut, M., Ataide, S.F., Haag, A., and Ban, N. (2011). Science *331*, 730–736.

Svidritskiy, E., Brilot, A.F., Koh, C.S., Grigorieff, N., and Korostelev, A.A. (2014). Structure *22*, 1210–1218.